A Cantilever Sensor With an Integrated Optical Readout for Detection of Enzymatically Produced Homocysteine

Stephan T. Koev, Rohan Fernandes, William E. Bentley, and Reza Ghodssi, *Member, IEEE*

Abstract—Microcantilever sensors have been recognized as a promising sensor platform for various chemical and biological applications. One of their major limitations is that the measurement of cantilever displacement typically involves elaborate off-chip setups with free-space optics. An improved device, known as the optical cantilever, has been proposed recently to eliminate the external optics. The response of the optical cantilever is measured on-chip through integrated waveguides. However, this method has been previously demonstrated only for devices operating in air, whereas most chemical and biological samples are in solution state. We present the first optical cantilever capable of operation in liquid. We test it with the detection of homocysteine with a minimal concentration of 10 μM. The minimal measurable cantilever displacement and surface stress are 5 nm and 1 mN/m, respectively. The presented device will be used in studies of a homocysteine-producing bacterial pathway for the purpose of drug discovery. It can also be extended to various other chemical- or biological-sensing applications by selecting an appropriate surface coating.

Index Terms—Cantilever sensor, enzyme, homocysteine, integrated waveguides.

I. INTRODUCTION

MICROCANTILEVERS have become popular in the field of miniaturized biological and chemical sensing [1]–[3]. They are compatible with microelectromechanical system (MEMS) batch processing, allowing dense arrays of devices to be fabricated in parallel at low cost. They detect samples in a label-free state and can be adapted for a wide range of applications. Microcantilevers have two sensing modes: 1) static and 2) dynamic. In the static mode, the target analyte causes beam bending due to increased surface stress. In the dynamic mode, the analyte causes a shift in the beam's resonant frequency due to the increased mass loading. For both modes of operation, it is necessary to measure the displacement of the cantilever as a function of time. The measurement typically employs an elaborate free-space optical setup using either a position-sensitive detector [4]–[7] or an interferometer [8], [9]. This off-chip setup is many orders of magnitude larger and more costly than the actual cantilever chip, and it can only measure one device at a time. Therefore, the advantages of the cantilever sensor are severely limited by the characteristics of the external readout setup.

Recently, a new cantilever design has been demonstrated that uses integrated optical waveguides for displacement measurement instead of external optics [10]–[12]. This device, known as the optical cantilever, is based on the principle of variable light coupling. The cantilever is part of an input waveguide which is butt-coupled to a fixed output waveguide. As the cantilever moves up or down, the amount of light coupled from the input to the output waveguide changes. This change serves as an indirect measure of the cantilever displacement. The optical cantilever method still requires an external laser to launch light into the on-chip waveguides and an external photodiode to collect it. However, these components are much smaller in size and cost than the free-space optical setup discussed before. As a result, the integrated waveguide readout can lead to low-cost, portable cantilever sensors with minimal off-chip complexity.

Previous work on the optical cantilever method was at the proof-of-concept stage, and there was no detection of an actual sample [10]–[12]. The reported devices were tested only in air and were not shown to be compatible with liquids. The majority of chemical and biological samples are in the solution state; therefore, the capability of the sensor to operate in liquid is crucial. In this paper, we report for the first time an optical cantilever sensor working in liquid in the static mode. To enable the operation in liquid, we embedded the cantilever inside a microfluidic channel. We also devised a method to overcome the stiction of the cantilever to the substrate, which normally occurs when microstructures are dried after wetting.

Previous demonstrations of the optical cantilever did not have a surface coating responsive to a particular sample [10]–[12]. Plain cantilevers (measured with external optics) are typically coated with a gold layer, which is functionalized with thiol-labeled probe biomolecules [1], [3], [13]. However, the previously reported optical cantilevers did not have a gold coating, possibly due to the issues of residual stress and optical loss. A metal layer on top of the cantilever can potentially bend it and misalign it from the output waveguide, preventing light from being coupled. In this paper, we add a gold layer on top of the optical cantilever that is very thin and does not significantly affect the
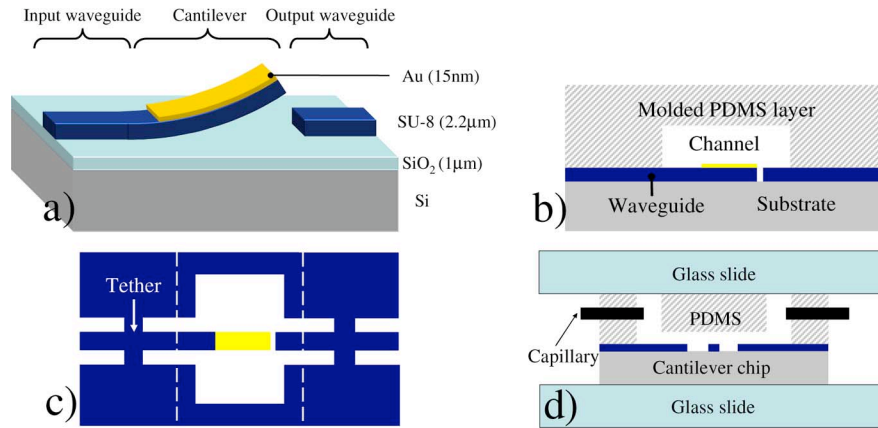
Fig. 1. (a) Schematic of optical cantilever. (b) Cross section of fluidic channel along the waveguide. (c) Top-down view of the SU-8 layer (dashed lines indicate channel location). (d) Cross section of assembled package along the fluidic channel.

cantilever bending or optical loss. This improvement enables the optical cantilever to be functionalized with probe biomolecules by the conventional thiol-labeling methods.

The optical cantilever reported here is used for the detection of homocysteine. The homocysteine molecule has a free thiol group at one end, which binds to the gold coating and causes surface stress and beam bending. This work is part of a broader project aimed at studying bacterial quorum sensing in a lab-on-a-chip format [14]–[16]. It has been shown that infectious bacteria communicate with each other using signaling molecules called auto-inducers [17]. Understanding and controlling these signals could lead to greatly improved antimicrobial drugs based on inhibiting bacterial communication [18], [19]. Auto-inducers are difficult to detect, but homocysteine is a byproduct of the synthesis of one type of auto-inducer that is recognized as "universal" [20]. Homocysteine, therefore, can be used as an indicator of its presence in the synthesis process. The homocysteine sensor will be a part of a microfluidic system used to test the effect of candidate drugs on bacterial communications.

II. CANTILEVER DESIGN

The optical cantilever in this paper was designed to sense in the static mode in order to facilitate operation in liquid. The dynamic mode cantilever detection in liquid has been demonstrated with free-space optics, but it is more challenging than the static mode due to the high viscous damping forces [5]. The wavelength of light used in the optical cantilever was chosen to be 635 nm due to the availability of low-cost red laser diodes. Most biological samples are dissolved in aqueous solutions, and water has very low absorbance at that wavelength [21].

A. Device Structure

A schematic of the optical cantilever with the relevant layer thicknesses is shown in Fig. 1(a). It consists of SU-8 polymer waveguides with SiO_2 bottom cladding on a Si substrate. The cantilever is a section of the input waveguide that is released from the SiO_2 surface and is coated with an Au layer. It bends up slightly due to residual stress gradient in the SU-8 and is vertically offset from the output waveguide by approximately

2 μm. The effect of this offset on the light coupling and sensitivity to displacement is discussed later. The horizontal gap between the cantilever and the output waveguide is 4 μm. Cantilevers with varying lengths were fabricated (70 μm, 110 μm, and 140 μm), whereas the width was fixed at 23 μm. The input and output waveguides are 1 cm long each. The light is coupled to and from the on-chip waveguides via optical fibers mounted on XYZ positioning stages.

The microfluidic channel is formed by placing a molded polydimethylsiloxane (PDMS) polymer layer on top of the cantilever chip. Fig. 1(b) shows a cross section of the device along the waveguide, and Fig. 1(c) shows a top-down schematic of the SU-8 layer. The waveguide tethers are added to form a continuous seal between the SU-8 and PDMS surfaces around the channel. The channel width, height, and length are 500 μm, 100 μm, and 1 cm, respectively. The channel is connected to external tubing via steel capillaries. The PDMS layer and the cantilever chip are held together between two glass slides by custom-made clamps. Fig. 1(d) illustrates the fluidic package excluding the clamps.

The waveguide has different cladding materials along its length: SiO_2 ($n = 1.5$), PDMS ($n = 1.4$), and water ($n = 1.33$). In all cases, the refractive index of the SU-8 core ($n = 1.6$) is higher than that of the cladding, and the waveguiding condition is satisfied. However, there is an increased propagation loss in the tethers due to lateral light leakage from the waveguide and in the gold layer due to its imaginary refractive index. Each tether is 25 μm wide, and the gold-coated region is 200 μm wide. Due to the shortness of these lossy waveguide regions, the total optical loss through them is acceptable.

B. Optical Sensitivity

The theoretical change in output optical power as a function of cantilever displacement can be found by calculating the overlap integral of the waveguide modes. The electric-field distributions of the modes in a rectangular waveguide are of the form $E(x, y) = E_0 P(x)Q(y)$ [22]. The mode exiting the cantilever is shifted vertically due to the cantilever vertical offset d, and it diverges during propagation in the unguided medium. The divergence in the horizontal direction (x) is

negligible compared to that in the vertical direction (y) due to the large width to thickness ratio of the waveguide. Therefore, the propagated mode that arrives at the output waveguide has the form $E_1(x, y) = E_0 P(x) Q_1(y - d)$.

We define the coupling coefficient to be the fraction of the power exiting the cantilever that is captured by the output waveguide. It is a function of offset and can be found by the overlap integral

$$C(d) = \frac{\left(\int Q(y) Q_1^*(y - d) \partial y \right)^2}{\int Q(y) Q^*(y) \partial y \int Q_1(y) Q_1^*(y) \partial y}. \quad (1)$$

Using the planar waveguide approximation [23], we estimated that there are six different vertical mode profiles (3 TE and 3 TM) in the SU-8 waveguide. Each mode has a different coupling coefficient. The distribution of power among the modes is random since it depends on scattering from waveguide defects. We assume that most of the power is in the fundamental mode and, therefore, the contributions of the other modes to the coupling coefficient are negligible. This assumption is partly justified by the fact that higher order modes have higher propagation and coupling losses.

The waveguide was modeled in finite element software (COMSOL Multiphysics) to find the vertical profile of the fundamental mode. It was determined that the mode shape is closely approximated by (2), where $\omega_0 = 0.9$ μm is a beam waist parameter. Due to divergence in the medium between the cantilever and output waveguide, the mode broadens and adopts the shape given by (3). The broadening factor B can be found from the Gaussian beam propagation model [23]; here, $B \approx 1.13$. Using the described mode profiles, the coupling coefficient from (1) is simplified to

$$Q(y) = \exp\left(-\frac{y^2}{\omega_0^2} \right) \quad (2)$$

$$Q_1(y) = \exp\left(-\frac{y^2}{\omega_0^2 B^2} \right) \quad (3)$$

$$C(d) = \frac{2B}{B^2 + 1} \exp\left(-\frac{2d^2}{\omega_0^2 (1 + B^2)} \right). \quad (4)$$

Note that the coupling coefficient is an even function of the offset d. Therefore, the position of an optical cantilever cannot be uniquely determined from the optical power. The same $C(d)$ could result from a positive or negative offset. For this reason, the cantilever in our design is constrained to be above the output waveguide, making d always positive. This eliminates the sign ambiguity; an increase in output power can be interpreted as downward cantilever displacement (decrease in d) and vice-versa.

The expected coupling coefficient as a function of cantilever vertical offset (4) is plotted in Fig. 2 (solid line). We define the optical sensitivity of the cantilever as the change in output power per unit cantilever displacement. This quantity is given by the first derivative of the coupling function (C') and is plotted in Fig. 2 (dashed line). The sensitivity peaks near an offset of 0.7 μm, while it vanishes near 0 and above 2.5 μm. Since the fabrication of the cantilever allows some control of the initial offset, the device can be tuned for maximum sensitivity. However, the noise sources also need to be taken into account in choosing the optimal fabrication offset.
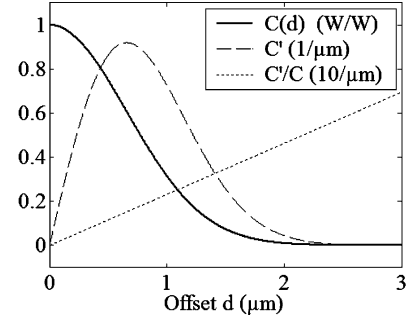

Fig. 2. Theoretical coupling function and optical sensitivity of cantilever for the fundamental mode.

In this paper, the optical cantilever operates in the static mode and the detector has a low bandwidth (1 Hz); consequently, the detector noise is very low. The main source of noise is the mechanical drift of the XYZ positioning stages that hold the fibers facing the input and output waveguides. This causes power fluctuations on the order of 2%. The power at the detector can be expressed by (5), where T is a fiber-to-waveguide coupling coefficient combined for both input and output, and the coefficient α accounts for the on-chip propagation loss. Changes in output power are caused either by the cantilever motion or by fiber-to-waveguide drift since P_{in} and α are fixed (6). This shows that decreasing the coupling coefficient $C(d)$ also decreases the drift noise. The signal-to-noise ratio (SNR) is approximated by (7), assuming that the fiber drift is the dominant source of noise. In that case, SNR is proportional to C'/C

$$P_{out} = P_{in} T C(d) \alpha \quad (5)$$

$$\Delta P_{out} = \Delta P_{cant} + \Delta P_{drft} = P_{in} \Delta C(d) T \alpha$$
$$+ P_{in} C(d) \Delta T \alpha \quad (6)$$

$$\text{SNR} \approx \frac{\Delta P_{cant}}{\Delta P_{drft}} = \frac{\Delta C}{C(d)} \frac{T}{\Delta T}$$
$$= \left(\frac{\partial C}{\partial d} \frac{1}{C(d)} \right) \frac{T}{\Delta T} \Delta d. \quad (7)$$

Fig. 2 shows that C'/C increases monotonically with the cantilever offset. Therefore, SNR can be improved by increasing the cantilever offset until drift noise becomes comparable to detector noise. The optimal offset depends on the contributions of each noise source and has not been determined exactly. We chose a target cantilever offset of 2.2 μm. We found that increasing the offset beyond 2.5 μm decreases the displacement signal too much, and the effects of stray light coupling and detector noise become significant.

C. Mechanical Sensitivity

We define the mechanical sensitivity of the cantilever as displacement Δd per unit surface stress $\Delta \sigma_s$. This quantity is given by the Stoney equation [24]

$$\frac{\partial d}{\partial \sigma_s} = 3 \frac{(1 - \nu)}{E} \left(\frac{L}{H} \right)^2. \quad (8)$$

Here, L and H are the cantilever length and thickness, respectively; E is the Young's modulus and ν is Poisson's ratio. Equation (8) shows that the mechanical sensitivity is improved by

TABLE I
CONTRIBUTIONS TO CURVATURE IN METAL- COATED SU-8 CANTILEVERS

Cause of curvature	Direction	Curvature (mm⁻¹)	Method to reduce curavture
Cross-linking gradient	up	$\mid k \mid < 0.1$	
- exposure dose gradient	down		Increase exposure dose
- temperature gradient	up		Bake in oven
E-beam evaporation	down	$\mid k \mid > 2$	Use thermal evaporation or sputtering
Cr layer residual stress	up	$\mid k \mid > 1.2$	Deposit Au without Cr layer
Swelling due to water	up	$0.23 < \mid k \mid < 0.37$	Increase hard bake time

reducing the thickness and increasing the length. The minimum thickness of SU-8 available at our fabrication facility is approximately 2 μm. The maximum length is limited to 150 μm due to the upward curvature of the cantilever, which will be discussed later. The Young's modulus of SU-8 (≈ 2 GPa) is two orders of magnitude lower than that of traditional cantilever materials, such as Si, Si_3N_4, SiO_2. Therefore, the use of SU-8 significantly improves the mechanical sensitivity for a given thickness.

III. FABRICATION

The fabrication of fixed optical waveguides requires materials with low loss and high refractive index of the core relative to the cladding. In addition, the fabrication of the cantilever waveguide requires a material with low residual stress gradient. The stress gradient causes the cantilever to curve and may prevent any power from being coupled to the output waveguide. It was shown above that a slight cantilever misalignment improves sensitivity, but it must be less than 2.5 μm and must be in the upward direction. We chose the cantilever material to be SU-8 since its residual stress is low and can be adjusted with the processing parameters.

A. Characterization of Curvature

Test structures were initially fabricated to evaluate the curvature of SU-8 beams for different processing conditions. These devices were similar to the reported optical cantilever but had a wide range of lengths, and the SiO_2 layer under the cantilever was removed. This allowed us to measure both downward and upward curvatures. The cantilever vertical offset was estimated either by depth measuring microscopy or by counting the number of interference fringes in the cantilever image (the second method will be explained later).

The residual stress in SU-8 is caused mainly by the thermal coefficient of expansion (CTE) mismatch between the substrate and the film [25], [26]. The cantilever offset depends on the residual stress gradient $\partial\sigma_r/\partial H$ in the SU-8 and is given by (9) [27]. The variables $d, \nu, E,$ and L were defined previously; k is the curvature of the cantilever (the reciprocal of radius of curvature)

$$d = \frac{(1-\nu)L^2}{2E}\left(\frac{\partial\sigma_r}{\partial H}\right) = \frac{kL^2}{2}. \qquad (9)$$

It has been suggested that the residual stress gradient in SU-8 results from a cross-linking gradient, which, in turn, is caused by exposure dose gradient and temperature gradient during processing [28]. The dose gradient and the temperature gradient create downward and upward cantilever bending, respectively. The former can be reduced by increasing the exposure dose sufficiently, and the latter can be minimized by baking in an oven instead of on a hotplate. For this application, cantilevers with a

slight upward curvature are required; therefore, we chose hotplate baking and tested different doses. Uncoated cantilevers with an upward curvature of approximately 0.1 mm-1 were obtained by using a dose of 200 mJ/cm^2. However, devices coated with gold had significantly increased curvature.

The deposition of 15-nm Au with a 15-nm Cr adhesion layer by e-beam evaporation resulted in a downward curvature exceeding 2 mm^{-1}. Etching the deposited metals did not eliminate the curvature, which suggests that the SU-8 acquires a residual stress gradient during the e-beam evaporation. We believe that heating or exposure to X-rays in the e-beam chamber creates a cross-linking gradient in the SU-8. Performing the metal deposition by sputtering or thermal evaporation eliminated this problem but resulted in large upward curvature of about 1.2 mm^{-1}.

Etching the deposited metals removed the upward curvature. This suggests that thermal evaporation and sputtering processes do not alter the SU-8 layer, but the metal films have residual stress. It was found that most of this residual stress is caused by the Cr adhesion layer. The deposition of 15 nm of Au directly on the SU-8 surface eliminated the upward curvature in dried cantilevers. The adhesion of Au to the SU-8 was excellent, and no delamination was observed throughout the testing. This may be due to the small thickness of the Au film.

An increased upward curvature was observed in Au-coated cantilevers immersed in water. We attributed this effect to swelling of the SU-8, which has also been noted elsewhere [29]. The top cantilever surface is blocked by metal and does not swell much, while the bottom surface is permeable to water and swells more. This creates a swelling gradient and beam bending. The swelling can be somewhat reduced by prolonged hard baking of the SU-8 at 190 °C, but that was found to increase the optical loss in the waveguide. The minimal curvature achieved for Au-coated cantilevers in water was approximately 0.23 mm^{-1}. Table I summarizes the different contributions to curvature that were discussed, and the next section describes the optimized fabrication process.

B. Fabrication Process

The fabrication of the optical cantilever begins with a 100-mm silicon wafer with [100] orientation. Thermal oxide is grown to a thickness of 1 μm. Next, a 30-nm-thick Cr film is deposited and patterned to serve as a sacrificial release layer for the cantilever. A 2.2-μm-thick layer of SU-8 5 epoxy (MicroChem Corp, USA) is spin-cast at 5200 r/min for 30 s. It is prebaked at 95 °C for 16 min; exposed in a contact aligner with a dose of 200 mJ/cm^2 at 365 nm; and post-baked at 95 °C for 16 min. The SU-8 is developed for 2 min and then hard baked at 190 °C for 45 min. All baking steps are performed on
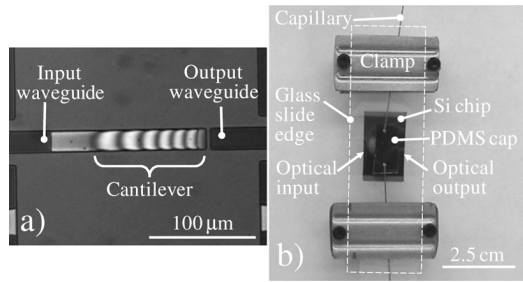
Fig. 3. (a) Microscope image (top-down view) of fabricated cantilever inside the fluidic channel. (b) Photograph of the assembled fluidic package.

a hotplate, and the temperature is ramped to the target value at 5 $^\circ$C/min. Next, a 15-nm-thick Au layer is deposited by thermal evaporation and patterned by liftoff. Finally, the cantilevers are released by immersing the wafer in Cr etchant-type TFD (Transene Inc, USA) for approximately 1 hr. This etchant is highly selective and does not attack the Au layer on top of the cantilever. The finished wafer is cleaved into chips with dimensions of approximately 2 cm $\times$ 1.5 cm, each containing eight cantilevers. The cleaved SU-8 waveguide facets are sufficiently smooth for optical coupling, provided that the waveguide pattern is closely aligned to the silicon cleaving plane during lithography.

Fig. 3(a) is a top-down image of a fabricated cantilever immersed in DI water. An interference pattern can be seen along the cantilever. This pattern is formed by light reflecting off the substrate and light reflecting off the cantilever surface. The thin Au layer is transparent, allowing light to pass through the cantilever. The number of interference fringes (minima or maxima) can be used as an estimate of the cantilever offset. Each fringe corresponds to half a wavelength. The image in Fig. 3(a) was obtained by using laser illumination with a free-space wavelength of 660 nm, which in water becomes 500 nm (assuming $n = 1.33$). There are seven interference fringes, resulting in an estimated offset of 1.7 μm. This method is used during testing to correlate the output optical power with cantilever displacement.

The PDMS capping layer is formed by using an SU-8 mold wafer. To fabricate the mold, a 100-μm-thick layer of SU-8 50 epoxy (MicroChem Corp, USA) is spin-cast onto a blank Si wafer and is patterned with the channel layout. The standard parameters provided by the manufacturer are used for the SU-8 50 processing. A PDMS mixture is prepared with 10:1 ratio of resin to curing agent (Sylgard 184, Dow Corning, USA). The SU-8 mold is placed in a 5-mm-deep dish, which is then completely filled with the PDMS mixture. The PDMS is cured at 80 $^\circ$C for 1 h. It is peeled off the mold and cut to a size slightly smaller than the cantilever chip. Vertical holes are made in the PDMS at the ends of the channel with a 1-mm drill bit. Then, steel capillaries (ID 200 μm, OD 400 μm) are inserted into the PDMS horizontally to meet these holes. Next, the PDMS layer with the capillaries is aligned on top of the cantilever chip while still wet, observing the alignment under a microscope. The chip and the PDMS are placed between two vertically stacked glass slides, which are compressed with clamps. The resulting spacing between the glass slides is approximately 5 mm, which allows external optical fibers to be inserted near the waveguide facets on the edge of the cantilever chip. The capillaries are connected to

Tygon flexible tubing (ID 380 μm, OD 2.3 mm), which is connected to a syringe pump for sample injection. Fig. 3(b) shows the fully assembled fluidic package.

C. Control of Stiction

Microstructures that are wetted and dried tend to adhere to the substrate. Cantilevers operating in air can be supercritically dried during the last fabrication step and never wetted again [11]. However, a cantilever for detecting liquid samples continues to be wetted and dried after fabrication and experiences stiction. We devised a method to release stuck cantilevers postpackaging by using the swelling behavior of SU-8. As previously discussed, metal-coated cantilevers have an upward curvature due to the swelling gradient of the SU-8 in water. This effect is greatly enhanced in solvents, such as methanol or IPA. Our method for releasing stuck cantilevers is to briefly flow methanol in the fluidic channel. The cantilever bends up and breaks away from the substrate. The methanol is followed by DI water, which relaxes the cantilever to a lower curvature and keeps it released.

IV. OPTICAL CHARACTERIZATION

The packaged device is mounted on a fixed stage under an optical microscope with a digital camera. A lensed 9-μm core fiber is used to couple light from a 635-nm pigtailed laser diode to the input waveguide. Light from the output waveguide is collected by a 62.5-μm core fiber and guided to a computer-controlled optical power meter. Both the input and output fibers are mounted on XYZ precision positioning stages.

The propagation loss in the waveguide was estimated by the scattered light intensity method [30]. The scattered light intensity along the waveguide was acquired from a digital image and fit to an exponential decay curve, giving a propagation loss of approximately 7 dB/cm.

The total loss in the system depends on the cantilever offset. The loss with the cantilever stuck to the substrate (i.e., zero offset) is on the order of 25 dB. This was measured by comparing the output fiber power (300 nW) to that in the input fiber (90 μW). Approximately 11 dB of the total loss is accounted for by propagation loss (total waveguide length is 1.5 cm), and the rest is attributed to a combination of fiber-to-waveguide coupling loss and cantilever coupling loss. The losses vary considerably from device to device, and the values listed here are representative but not exact.

We measured the output optical power for varying cantilever offsets in air. This was performed by drying an unpackaged cantilever and moving its tip vertically with a microprobe needle. The resulting cantilever offset was estimated by counting the number of interference fringes in the microscope image as described previously. Fig. 4 shows the measured power at each offset. The theoretical power based on the coupling function is plotted for comparison (the coupling function is scaled, making its peak equal to the maximum measured output power). Overall, the data points agree reasonably well with the theoretical curve. The discrepancies are most likely due to cantilever torsion. The microprobe needle used to move the cantilever vertically also twists it slightly; this should make the measured output power lower than the theoretical value.
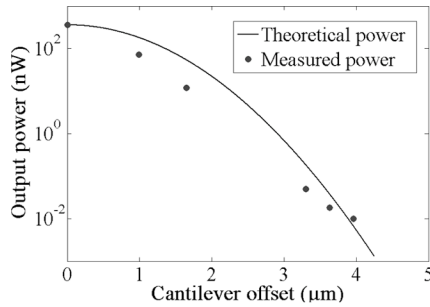
Fig. 4. Measured and theoretical optical output power versus offset for a 140-μm-long cantilever. The device is tested in an unpackaged, dried state.

Fig. 5. Response of an optical cantilever to 5-mM solution of homocysteine in DI water. The cantilever is 110 μm long and has a 2.2-μm initial offset.

V. HOMOCYSTEINE DETECTION

The packaged optical cantilever was tested by detection of homocysteine solutions. As discussed previously, homocysteine is a byproduct of the bacterial signaling pathway, and the capability to detect it in a microfluidic device will be useful for antibacterial drug discovery. Two types of homocysteine detection experiments were carried out to verify the sensor response. For the first experiment, we prepared homocysteine samples externally and introduced them into the device. For the second type of experiment, we functionalized the Tygon microfluidic tubing with bacterial enzymes; the homocysteine was synthesized in situ by these enzymes and detected by the cantilever downstream. All liquids were injected in the device by the external syringe pump at rates ranging from 2 μL/min to 10 μL/min. Before each experiment, the device was cleaned by flowing dilute HCl (1% v/v) for 5 min, followed by a DI water rinse for 5 min. The optical fibers were initially aligned to the input and output waveguides by adjusting the XYZ stages and were left in the same position for the whole experiment. The output of the optical power meter was continuously logged by a computer at a sampling frequency of 1 Hz.

The externally prepared samples were obtained by dissolving homocysteine powder (Sigma Aldrich, USA) in DI water. They were introduced in the device after flowing pure DI water to establish a baseline signal. Fig. 5 shows the response of the optical cantilever to a 5-mM externally prepared homocysteine solution. The coupled power increases by a factor of 9 over a period of 500 s after sample introduction due to gradual binding of homocysteine to the gold surface. The sample is followed by DI water, which does not appreciably change the output power. Ideally, no change in power is expected here since the thiol group of homocysteine should be covalently bound to the gold surface and should not be removed by water rinsing. The small decrease in power may be the result of some physically adsorbed homocysteine molecules being removed.

The DI water flowing before and after the homocysteine sample introduction has exactly the same optical properties. This verifies that the change in output power is caused by cantilever bending and not by a change in the optical properties of the medium. The shape of the coupling function (Fig. 2) suggests that the increase in output power in Fig. 5 was caused by downward cantilever displacement. This was confirmed by counting the number of interference fringes in the microscope image of the cantilever before and after the sample introduction. Downward displacement means that the homocysteine
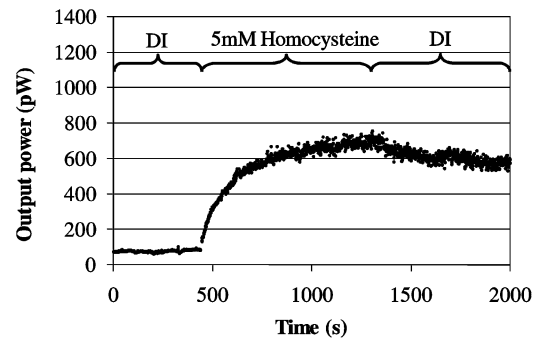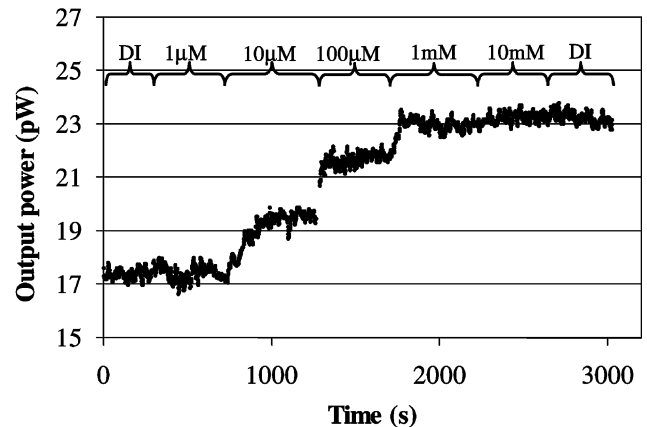

Fig. 6. Response of an optical cantilever to increasing concentrations of homocysteine. The cantilever is 70 μm long and has a 750-nm initial offset.

creates compressive stress on the gold surface. This conclusion is consistent with reports of the stress generated by other thiol compounds [6], [7].

Fig. 6 shows the response of an optical cantilever to increasing concentrations of homocysteine. Solutions with concentration from 1 μM to 10 mM were introduced sequentially. The lowest concentration does not produce a measurable change in optical power, but the second lowest (10 μM) causes a clear response. The optical power changes further by introducing 100-μM and 1-mM solutions, although the relative changes become smaller. Finally, the transition to 10 mM does not produce any measurable response.

These results are consistent with the first-order kinetics model of thiol assembly to gold surfaces [31]. According to the model, the final surface density of thiols is independent of the solution concentration, and the binding rate is proportional to the solution concentration and the vacant surface area. In the 1 μM region in Fig. 6, the solution concentration is the limiting factor to the binding rate. In the 10-mM region, the surface is already covered with thiols by the previous samples, and the vacant surface area becomes the limiting factor. This explains why the binding rate in both of these regions is low and the change of optical power is unmeasurable. However, the first-order thiol assembly model is a crude approximation. After the initial binding, the thiol layers undergo several phase transitions that are not completely understood [32]. For this reason, we were not able to perform a more quantitative analysis of the cantilever response
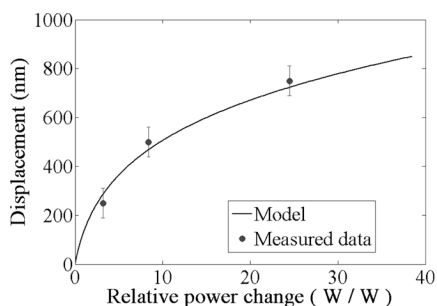
Fig. 7. Measured and theoretical displacement of a cantilever versus relative increase in optical power. The cantilever is 140 μm long and has 2.2-μm initial offset. It is tested in 5-mM homocysteine solution.

as a function of homocysteine concentration. Importantly, the study of bacterial quorum sensing that this device will be used for does not require concentration measurements. For this application, it is sufficient to detect the presence of homocysteine.

The cantilever displacement during homocysteine binding can be estimated by counting the number of interference fringes in the microscope image. Fig. 7 shows three estimated displacements versus the measured relative power increase (increase in power divided by initial power) for a 140-μm-long cantilever in response to 5-mM homocysteine. The three data points were obtained at different times after the sample introduction. The vertical error bars are due to the resolution limit of the fringe-counting measurement ($\sim$120 nm).

Fig. 7 also shows the theoretical relative power increase based on the coupling function. The curve was obtained by dividing the theoretical increase in coupling coefficient at varying displacements by the coupling coefficient at the initial offset. The initial offset used in this calculation was estimated by the fringe counting method. The measured data in Fig. 7 agree reasonably well with the model. This suggests that the model can be used to translate changes of output power into cantilever displacement. The model can be extended to cantilevers with different lengths and initial offsets.

The second type of homocysteine experiment was performed by using bacterial enzymes in the microfluidics tubing to synthesize homocysteine *in situ*. The synthetic pathway of the bacterial signaling molecule AI-2 consists of the enzymes Pfs and LuxS [19], [20]. Pfs converts the compound S-adenosyl homocysteine (SAH) into S-ribosyl homocysteine (SRH), and LuxS converts SRH into AI-2 and homocysteine. The homocysteine can serve as an indicator of AI-2 in studies of bacterial quorum sensing.

Fernandes *et al.* synthesized the enzymes Pfs and LuxS and used them to convert SAH into AI-2 and homocysteine in vitro [15], [16]. The enzymes were assembled on chitosan-coated magnetic nanoparticles for controlled delivery to bacterial cells. In the present work, we use the same enzymatic nanoparticles and immobilize them in the microfluidic tubing at the input of the optical cantilever package. SAH solutions entering the device are converted into homocysteine, which is detected downstream by the cantilever.

Enzyme-coated magnetic nanoparticles were prepared as described in [16]. The nanoparticle solution was injected into a 10-cm-long Tygon tube. A magnetic field was applied perpendicular to the tube with a permanent magnet for 5 min, forming a
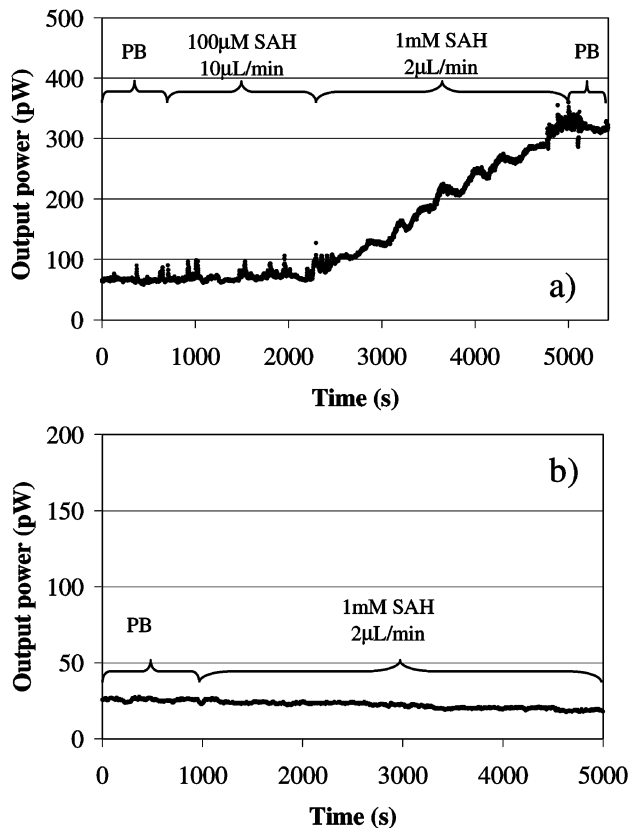

Fig. 8. (a) Response of an optical cantilever to SAH introduction; the input tubing is functionalized with Pfs and LuxS enzymes. (b) Response of an optical cantilever to SAH introduction; there are no enzymes in the tubing. Both cantilevers are 110 μm long and have 2.2-μm initial offset.

visible film of particles adsorbed on the inner walls. The magnet was removed, and the tube was rinsed with DI water to remove any loosely bound particles form the walls. A visible film of adsorbed particles remained even after extensive rinsing. The functionalized tube was attached to the input capillary of the optical cantilever package.

An SAH solution was prepared by dissolving SAH powder in 10–mM sodium phosphate buffer (PB) with a pH of 5.9. The solution was introduced into the device after flowing PB for 10 min to establish a baseline signal. Fig. 8(a) shows the optical response of the cantilever to the SAH for two different concentration and flow–rate conditions. The concentration of homocysteine near the cantilever depends on the SAH concentration and the residence time of SAH at the enzymes, which is inversely proportional to the flow rate. In Fig. 8(a), the cantilever response to 100 μM SAH flowing at 10 μL/min is undetectable. However, increasing the concentration to 1 mM and reducing the flow rate to 2 μL/min causes a measurable change in power.

We also performed an SAH experiment using a device whose microfluidic input tubing was not functionalized with enzymatic particles. Fig. 8(b) shows the optical response of this cantilever to 1 mM SAH flowing at 2 μL/min. There is a slight downward trend in the power, probably caused by XYZ stage drift; however, there are no major changes upon the injection of SAH. Therefore, the cantilever in Fig. 8(a) does not respond to the SAH itself but to the homocysteine produced by the enzymes.

This result is expected since SAH does not have free thiol groups that could bind to the cantilever surface.

VI. DISCUSSION

The cantilever displacement in each experiment can be estimated from the measured power change based on the theoretical coupling function and the measured initial cantilever offset. The results in Fig. 7 show that the displacement obtained by this method is in good agreement with the displacement measured by fringe counting. Further, the displacement can be used to calculate homocysteine-induced surface stress based on the mechanical sensitivity of the cantilever.

The maximum relative increases in optical power in Figs. 5–8 are 8, 0.3, 24, and 3.6, respectively. Using the theoretical coupling function and measured initial offset of each cantilever, we found that these power changes correspond to displacements of 440 nm, 150 nm, 750 nm, and 300 nm. Using the mechanical sensitivity for each cantilever, we calculated the surface stress to be 0.17 N/m, 0.14 N/m, 0.17 N/m, and 0.11 N/m, respectively. These stress values are in reasonable agreement. Some variation between devices is to be expected since the thiol layer density depends on gold surface properties [32]. Interestingly, stresses in the range of 0.08 N/m to 0.25 N/m have been reported for several thiol compounds with varying chain lengths [7]. The measured values for homocysteine here are on the same order of magnitude.

The minimal detectable displacement of the cantilever depends on the noise power. The variation of the baseline signal before sample injection is on the order of 2% of the coupled power. Therefore, the minimal measurable relative change in power caused by a sample is approximately 0.02. According to the model described in Fig. 7, this power change corresponds to a minimal detectable displacement of 5 nm. Considering the mechanical sensitivity (8), the minimal surface stress that can be detected with the cantilever is 1 mN/m. This is a considerable improvement over previous work, where the minimal detectable stress was 200 mN/m [10].

We believe that the main source of variations in the baseline signal is the drift of the XYZ fiber positioning stages. The minimal detectable cantilever displacement can be lowered by improving the method of coupling light to and from the on-chip waveguides.

A technology for bonding lasers and photodiodes to Si substrates (known as hybrid integration) has been developed previously for optical-communications applications [33], [34]. The same approach can be used here to couple light to and from the on-chip waveguides permanently without the need for XYZ stages. This would decrease the power drift and improve the minimal detectable cantilever displacement. Moreover, it would reduce the size of the measurement setup and result in a more compact, low-cost sensor that can be used in an array format.

VII. CONCLUSION

We present the first optical cantilever sensor capable of detecting liquid samples. The optical cantilever is a beam whose displacement is measured through integrated optical waveguides. This method improves on the traditional techniques for beam displacement measurements since it does not require elaborate free-space optics. In addition, it does not require

top-down optical access to the cantilever, allowing for greater flexibility in the selection of packaging materials.

The device presented here has several advantages over the previous demonstrations of optical cantilevers. First, it is embedded inside a microfluidic channel for transporting the liquid sample. In case of stiction with the substrate, it can be released by exploiting the swelling behavior of SU-8 in methanol. Second, the cantilever has a gold surface layer that can be functionalized with thiol-labeled biomolecules. Third, the cantilever forms an interference pattern, which can be used for independent measurement of displacement. Fourth, the cantilever is constrained to be always above the output waveguide. This eliminates the ambiguity which occurs if the cantilever is free to move on both sides of the output.

A theoretical model for cantilever optical coupling as a function of offset was developed and used to predict the impact of misalignment on sensitivity. The fabrication process was tuned to minimize the cantilever curvature while allowing a slight offset from the output waveguide. The coupling model was found to be in reasonable agreement with the experimental results.

The completed optical cantilever was tested by detecting homocysteine, which is a thiol-containing compound found in bacterial signaling pathways. The device will be used in microfluidics-based studies of bacterial quorum sensing. However, it can be readily extended to other more traditional cantilever applications, such as DNA hybridization assays and immunoassays. We believe that the combination of a cantilever sensor with integrated optics and a microfluidic channel presented here is a significant addition to the lab-on-a-chip toolbox.

REFERENCES

[1] N. V. Lavrik, M. J. Sepniak, and P. G. Datskos, "Cantilever transducers as a platform for chemical and biological sensors," *Rev. Sci. Instrum.*, vol. 75, pp. 2229–2253, 2004.

[2] H. P. Lang, M. Hegner, E. Meyer, and C. Gerber, "Nanomechanics from atomic resolution to molecular recognition based on atomic force microscopy technology," *Nanotechnology*, vol. 13, pp. R29–R36, 2002.

[3] L. G. Carrascosa, M. Moreno, M. Alvarez, and L. M. Lechuga, "Nanomechanical biosensors: A new sensing tool," *TrAC, Trends Anal. Chem.*, vol. 25, pp. 196–206, 2006.

[4] R. McKendry, J. Zhang, Y. Arntz, T. Strunz, M. Hegner, H. P. Lang, M. K. Baller, U. Certa, E. Meyer, H.-J. Guntherodt, and C. Gerber, "Multiple label-free biodetection and quantitative DNA-binding assays on a nanomechanical cantilever array," in *Proc. Nat. Acad. Sci. USA*, 2002, vol. 99.

[5] T. Braun, V. Barwich, M. K. Ghatkesar, A. H. Bredekamp, C. Gerber, M. Hegner, and H. P. Lang, "Micromechanical mass sensors for biomolecular detection in a physiological environment," *Phys. Rev. E*, vol. 72, 2005.

[6] M. Calleja, J. Tamayo, A. Johansson, P. Rasmussen, L. Lechuga, and A. Boisen, "Polymeric cantilever arrays for biosensing applications," *Sens. Lett.*, vol. 1, pp. 1–5, 2003.

[7] R. Berger, E. Delamarche, H. P. Lang, C. Gerber, J. K. Gimzewski, E. Meyer, and H.-J. Güntherodt, "Surface stress in the self-assembly of alkanethiols on gold probed by a force microscopy technique," *Appl. Phys. A*, vol. 66, pp. S55–S59, 1998.

[8] S. T. Koev, M. A. Powers, H. Yi, L.-Q. Wu, W. E. Bentley, G. W. Rubloff, G. F. Payne, and R. Ghodssi, "Mechano-transduction of DNA hybridization and dopamine oxidation through electrodeposited chitosan network," *Lab Chip*, vol. 7, pp. 103–111, 2007.

[9] M. Helm, J. J. Servant, F. Saurenbach, and R. Berger, "Read-out of micromechanical cantilever sensors by phase shifting interferometry," *Appl. Phys. Lett.*, vol. 87, pp. 064101–064101, 2005.

[10] M. Nordström, D. A. Zauner, M. Calleja, J. Hübner, and A. Boisen, "Integrated optical readout for miniaturization of cantilever-based sensor system," *Appl. Phys. Lett.*, vol. 91, pp. 103512–103512, 2007.

[11] M. W. Pruessner, N. Siwak, K. Amarnath, S. Kanakaraju, W.-H. Chuang, and R. Ghodssi, "End-coupled optical waveguide MEMS devices in the indium phosphide material system," *J. Micromech. Microeng.*, vol. 16, pp. 832–842, 2006.

[12] K. Zinoviev, C. Dominguez, J. A. Plaza, V. J. C. Busto, and L. M. Lechuga, "A novel optical waveguide microcantilever sensor for the detection of nanomechanical forces," *J. Lightw. Technol.*, vol. 24, no. 5, pp. 2132–2138, May 2006.

[13] R. Raiteri, M. Grattarola, H.-J. Butt, and P. Skladal, "Micromechanical cantilever-based biosensors," *Sens. Actuators, B*, vol. 79, pp. 115–126, 2001.

[14] X. Luo, A. T. Lewandowski, H. Yi, G. F. Payne, R. Ghodssi, W. E. Bentley, and G. W. Rubloff, "Programmable assembly of a metabolic pathway enzyme in a pre-packaged reusable bioMEMS device," *Lab Chip*, vol. 8, pp. 420–430, 2008.

[15] R. Fernandes, C. Y. Tsao, Y. Hashimoto, L. Wang, T. K. Wood, G. F. Payne, and W. E. Bentley, "Magnetic nanofactories: Localized synthesis and delivery of quorum-sensing signaling molecule autoinducer-2 to bacterial cell surfaces," *Metab. Eng.*, vol. 9, pp. 228–239, 2007.

[16] R. Fernandes and W. Bentley, "AI-2 biosynthesis module in a magnetic nanofactory alters bacterial response via localized synthesis and delivery," *Biotechnol. Bioeng.*, vol. 102, pp. 390–399, 2009.

[17] J. C. March and W. E. Bentley, "Quorum sensing and bacterial crosstalk in biotechnology," *Curr. Opin. Biotechnol.*, vol. 15, pp. 495–502, 2004.

[18] M. Hentzer and M. Givskov, "Pharmacological inhibition of quorum sensing for the treatment of chronic bacterial infections," *J. Clin. Invest.*, vol. 112, pp. 1300–1307, 2003.

[19] A. Vendeville, K. Winzer, K. Heurlier, C. M. Tang, and K. R. Hardie, "Making 'sense' of metabolism: Autoinducer-2, LuxS and pathogenic bacteria," *Nat. Rev. Microbiol.*, vol. 3, pp. 383–396, 2005.

[20] K. B. Xavier and B. L. Bassler, "LuxS quorum sensing: More than just a numbers game," *Curr. Opin. Microbiol.*, vol. 6, pp. 191–197, 2003.

[21] G. M. Hale and M. R. Querry, "Optical constants of water in the 200-nm to 200-mm wavelength region," *Appl. Opt.*, vol. 12, pp. 555–563, 1973.

[22] R. G. Hunsperger, *Integrated Optics*. Berlin, Germany: Springer-Verlag, 2002.

[23] B. E. A. Saleh and M. C. Teich, *Fundamentals of Photonics*. New York: Wiley, 1991.

[24] Y. Zhang, Q. Ren, and Y.-P. Zhao, "Modelling analysis of surface stress on a rectangular cantilever beam," *J. Phys. D: Appl. Phys.*, vol. 37, pp. 2140–2145, 2004.

[25] R. Feng and R. J. Farris, "Influence of processing conditions on the thermal and mechanical properties of SU8 negative photoresist coatings," *J. Micromech. Microeng.*, vol. 13, pp. 80–88, 2003.

[26] D. Bachmann, B. Schoberle, S. Kuhne, Y. Leiner, and C. Hierold, "Fabrication and characterization of folded SU-8 suspensions for MEMS applications," *Sens. Actuators, A*, vol. 130–131, pp. 379–386, 2006.

[27] J.-A. Schweitz and F. Ericson, "Evaluation of mechanical materials properties by means of surface micromachined structures," *Sens. Actuators, A*, vol. 74, pp. 126–133, 1999.

[28] D. Sameoto, S.-H. Tsang, I. G. Foulds, S.-W. Lee, and M. Parameswaran, "Control of the out-of-plane curvature in SU-8 compliant microstructures by exposure dose and baking times," *J. Micromech. Microeng.*, vol. 17, pp. 1093–1098, 2007.

[29] G. C. Hill, R. Melamud, F. E. Declercq, A. A. Davenport, I. H. Chan, P. G. Hartwell, and B. L. Pruitt, "SU-8 MEMS Fabry-Perot pressure sensor," *Sens. Actuators, A*, vol. 138, pp. 52–62, 2007.

[30] B. M. Foley, P. Melman, and K. T. Vo, "Novel loss measurement technique for optical waveguides by imaging of scattered light," *Electron. Lett.*, vol. 28, pp. 584–585, 1992.

[31] R. F. DeBono, G. D. Loucks, D. D. Manna, and U. J. Krull, "Self-assembly of short and long-chain n-alkyl thiols onto gold surfaces: A real-time study using surface plasmon resonance techniques," *Can. J. Chem.*, vol. 74, pp. 677–688, 1996.

[32] F. Schreiber, "Self-assembled monolayers: From 'simple' model systems to biofunctionalized interfaces," *J. Phys.: Condens. Matter*, vol. 16, pp. R881–R900, 2004.

[33] T. Hashimoto, Y. Nakasuga, Y. Yamada, H. Terui, M. Yanagisawa, Y. Akahori, Y. Tohmori, K. Kato, and Y. Suzuki, "Multichip optical hybrid integration technique with planar lightwave circuit platform," *J. Lightw. Technol.*, vol. 16, no. 7, pp. 1249–1258, Jul. 1998.

[34] C. A. Jones and K. Cooper, "Hybrid integration onto silicon motherboards with planar silica waveguides," in *Proc. Inst. Elect. Eng., Optoelectron.*, 1996, vol. 143.

Stephan T. Koev was born in Bulgaria in 1981. He received the B.S. degree in electrical engineering from the U.S. Naval Academy, Annapolis, MD, in 2004 and the M.S. and Ph.D. degrees in electrical engineering from the University of Maryland, College Park, in 2007 and 2009, respectively.

His doctoral research was in the area of microelectromechanical systems (MEMS) for biomedical applications. He developed optical readout methods for microcantilever sensors and integrated them with microfluidics. His broader interests include micro- or nanofabrication, integrated optics, biodevice interfaces, and MEMS metrology. Currently, he is a Postdoctoral Research Associate with the Center for Nanoscale Science and Technology at the National Institute of Standards and Technology, Gaithersburg, MD.

Rohan Fernandes was born in India. He received the B.Sc. degree in chemical engineering from the Institute of Chemical Technology (formerly UDCT), Mumbai, India in 2001, the M.S. degree in chemical and biochemical engineering from the University of Maryland, Baltimore County (UMBC), in 2003, and the Ph.D. degree in bioengineering from the University of Maryland, College Park, in 2008.

Currently, he is a Postdoctoral Fellow in the Chemical and Biomolecular Engineering Department at Johns Hopkins University, Baltimore, MD. His research interests include nanobiotechnology, drug delivery devices, and microfluidics devices for biotechnological applications.

William E. Bentley received the B.S. and M.S. degrees in chemical engineering from Cornell University, Ithaca, NY, and the Ph.D. degree in chemical engineering from the University of Colorado, Boulder.

Currently, he is the Robert E. Fischell Distinguished Professor and Chair of the Fischell Department of Bioengineering at the University of Maryland. He holds joint appointments with the Maryland Technology Enterprise Institute (MTECH) and the University of Maryland Biotechnology Institute. His research interests include biomolecular and metabolic engineering, cell-to-cell communication, heterologous protein expression, and device/bio interfaces.

Dr. Bentley is a Fellow of the American Institute of Medical and Biological Engineers, the American Association for the Advancement of Science, and the American Academy of Microbiology.

Reza Ghodssi (M'96) is the Herbert Rabin Distinguished Professor and Director of the MEMS Sensors and Actuators Lab (MSAL) in the Department of Electrical and Computer Engineering (ECE) and the Institute for Systems Research (ISR) at the University of Maryland (UMD), College Park. He is also affiliated with the Fischell Department of Bioengineering (BIOE), the Maryland NanoCenter, the UMD Energy Research Center (UMERC), and the Materials Science and Engineering Department (MSE) at UMD. His research interests are the design and development of microfabrication technologies and their applications to micro/nanodevices and systems for chemical and biological sensing and small-scale energy conversion and harvesting. He has more than 68 scholarly publications, is co-editor of the "Handbook of MEMS Materials and Processes" to be published in 2009, and is an Associate Editor for the *Journal of Micorelectromechanical Systems* (JMEMS) and Biomedical Microdevices (BMMD).

Dr. Ghodssi received the 2001 UMD George Corcoran Award, the 2002 National Science Foundation CAREER Award, and the 2003 UMD Outstanding Systems Engineering Faculty Award. Dr. Ghodssi is the Chair of the 9th International Workshop on Micro and Nanotechnology for Power Generation and Energy Conversion Applications, also known as "PowerMEMS 2009," co-founder of MEMS Alliance in the greater Washington area, and a member of the American Vacuum Society, Materials Research Society, American Society for Engineering Education, and the American Association for the Advancement of Science.